

Magnetic resonance imaging of glutamate

Kejia Cai^{1,4}, Mohammad Haris^{1,4}, Anup Singh^{1,4}, Feliks Kogan¹, Joel H Greenberg², Hari Hariharan¹, John A Detre¹⁻³ & Ravinder Reddy¹

Glutamate, a major neurotransmitter in the brain, shows a pH- and concentration-dependent chemical exchange saturation transfer effect (GluCEST) between its amine group and bulk water, with potential for *in vivo* imaging by nuclear magnetic resonance. GluCEST asymmetry is observed ~3 p.p.m. downfield from bulk water. Middle cerebral artery occlusion in the rat brain resulted in an ~100% elevation of GluCEST in the ipsilateral side compared with the contralateral side, predominantly owing to pH changes. In a rat brain tumor model with blood-brain barrier disruption, intravenous glutamate injection resulted in a clear elevation of GluCEST and a similar increase in the proton magnetic resonance spectroscopy signal of glutamate. GluCEST maps from healthy human brain were also obtained. These results demonstrate the feasibility of using GluCEST for mapping relative changes in glutamate concentration, as well as pH, *in vivo*. Contributions from other brain metabolites to the GluCEST effect are also discussed.

Glutamate and γ -aminobutyric acid (GABA) are the major excitatory and inhibitory neurotransmitters, respectively, in the brain and are likely involved in nearly all signal processing functions of the central nervous system (CNS) and altered in many CNS diseases¹⁻⁴. Magnetic resonance imaging (MRI) is a noninvasive imaging technique that provides exquisite structural detail, but current MRI methods are not capable of imaging the distribution of neurotransmitters in brain (**Supplementary Note**).

Proton magnetic resonance spectroscopy (¹H MRS) can detect several neurotransmitter signature groups using a variety of techniques⁵⁻¹⁰. However, ¹H MRS techniques require long acquisition times and have poor spatial resolution. Here we describe a new MRI technique for imaging glutamate (R.R., K.C., M.H., A.S., F.K. and H.H., unpublished data) based on its chemical exchange saturation transfer (CEST) effect¹¹⁻¹⁵. GluCEST provides markedly higher spatial and temporal resolution compared with ¹H MRS. The CEST effect from amide and hydroxyl protons from different amino acids, proteins and other molecules^{12,16,17} have previously been exploited to measure pH *in vivo*^{18,19}, glycogen in the liver²⁰, glycosaminoglycans in cartilage²¹, gene expression *in vivo*²² and myo-inositol in brain²³, but no prior studies have used the CEST effect of amine protons to image glutamate *in vivo*.

Here the pH and concentration dependence of GluCEST is first demonstrated *in vitro* at 37 °C. Second, the feasibility of measuring

GluCEST *in vivo* from rat brain with and without focal ischemia is shown. Third, changes in GluCEST and glutamate ¹H MRS in response to exogenous injection of glutamate in a rat brain tumor model are compared. Finally, the feasibility of mapping the glutamate signal from healthy human brain *in vivo* is demonstrated at 7 Tesla (7T), an ultrahigh-field whole-body imaging scanner. The potential contributions to GluCEST from other brain metabolites, as well as the advantages and shortcomings of this approach, are also discussed.

RESULTS

Phantom studies

The z-spectra of 10 mM glutamate solutions at varying pHs (phantoms) demonstrate that at lower pHs (pH < 6.0), the CEST peak of glutamate is sharper and centered around 3 p.p.m. higher frequency from the bulk water resonance (absolute chemical shift, 7.7 p.p.m.) (**Fig. 1a**). The z-spectral asymmetry plots (**Fig. 1b**) gave a broad CEST effect ranging from 1 to 4 p.p.m. relative to bulk water resonance. Whereas the GluCEST asymmetry plots from low pH solutions showed clear peaks centered at ~3.00 p.p.m., the peak position of asymmetry plots from higher pH solutions (pH > 6.0) gradually moved toward that of water resonance. At pH 7, the maximum of the asymmetry plot occurred at ~1.2 p.p.m., and its amplitude was ~100% higher than at 3 p.p.m. This is the well known phenomenon of intermediate- to fast-exchange ($k \geq \Delta\omega$)-mediated chemical shift averaging. Despite the shift in peak position at pH 7, all of our studies reported here used 3 p.p.m. as the GluCEST resonance saturation frequency to maintain consistency.

Because of non-steady-state experimental conditions, we analyzed the sensitivity of GluCEST by solving numerical simulations of full Bloch-McConnell equations²⁴ using the experimental parameters from these studies. We found an excellent agreement between the experimental z-spectral asymmetry curves and numerically simulated ones. Because the intracellular pH in the brains of normal healthy volunteers is reported to be ~7.0 (ref. 25), the GluCEST contrast at this pH is the most relevant for *in vivo* imaging. On the basis of the fitted z-spectral asymmetry curve from simulations (**Fig. 1b**), the amine-proton exchange rate (k) in a 10 mM glutamate solution (pH 7.0) at 37 °C was estimated to be in the range of $5,500 \pm 500 \text{ s}^{-1}$. This is comparable to the chemical shift difference ($\Delta\omega$) at 7T ($\Delta\omega = 5,700 \text{ rad s}^{-1}$); thus, GluCEST imaging is feasible at 7T, as well as at higher field strengths.

¹Center for Magnetic Resonance and Optical Imaging, Department of Radiology, University of Pennsylvania, Philadelphia, Pennsylvania, USA. ²Department of Neurology, University of Pennsylvania, Philadelphia, Pennsylvania, USA. ³Center for Functional Neuroimaging, Department of Radiology, University of Pennsylvania, Philadelphia, Pennsylvania, USA. ⁴These authors contributed equally to this work. Correspondence should be addressed to R.R. (ravi@mail.mmrrcc.upenn.edu).

Received 14 December 2010; accepted 2 August 2011; published online 22 January 2012; doi:10.1038/nm.2615

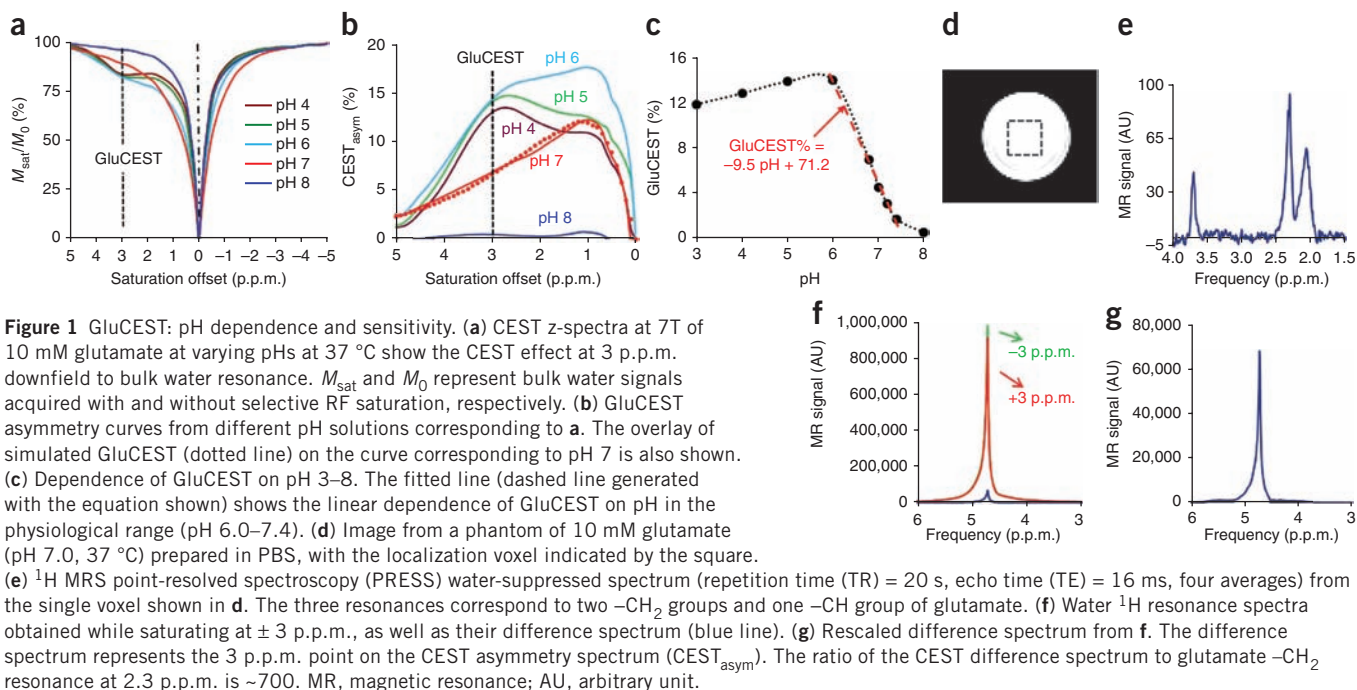


Figure 1 GluCEST: pH dependence and sensitivity. (a) CEST z-spectra at 7T of 10 mM glutamate at varying pHs at 37 °C show the CEST effect at 3 p.p.m. downfield to bulk water resonance. M_{sat} and M_0 represent bulk water signals acquired with and without selective RF saturation, respectively. (b) GluCEST asymmetry curves from different pH solutions corresponding to a. The overlay of simulated GluCEST (dotted line) on the curve corresponding to pH 7 is also shown. (c) Dependence of GluCEST on pH 3–8. The fitted line (dashed line generated with the equation shown) shows the linear dependence of GluCEST on pH in the physiological range (pH 6.0–7.4). (d) Image from a phantom of 10 mM glutamate (pH 7.0, 37 °C) prepared in PBS, with the localization voxel indicated by the square. (e) ^1H MRS point-resolved spectroscopy (PRESS) water-suppressed spectrum (repetition time (TR) = 20 s, echo time (TE) = 16 ms, four averages) from the single voxel shown in d. The three resonances correspond to two $-\text{CH}_2$ groups and one $-\text{CH}$ group of glutamate. (f) Water ^1H resonance spectra obtained while saturating at ± 3 p.p.m., as well as their difference spectrum (blue line). (g) Rescaled difference spectrum from f. The difference spectrum represents the 3 p.p.m. point on the CEST asymmetry spectrum (CEST_{asym}). The ratio of the CEST difference spectrum to glutamate $-\text{CH}_2$ resonance at 2.3 p.p.m. is ~ 700 . MR, magnetic resonance; AU, arbitrary unit.

Whereas it is possible to achieve a higher GluCEST sensitivity by using higher B_1 , the imaging parameters chosen here were constrained by the exchange rate differences between phantoms and *in vivo* tissue, as well as RF-specific absorption rate (SAR) issues in human studies at 7T. As SAR is proportional to the B_1^2 , and the square of the static magnetic field (B_0^2), the allowed B_1 amplitude at 7T is limited for human imaging.

Potential contributions from other brain metabolites

The major metabolites in the brain visible with ^1H MRS at physiological concentrations are *N*-acetyl aspartate, choline, myo-inositol, creatine, glutamine, taurine, aspartate, glutamate and GABA. After investigating the CEST properties from each of these metabolites in phantoms, we found that, with the experimental parameters used here, except for a small contribution from GABA and creatine, all other metabolites contributed negligible CEST effects to GluCEST (Fig. 2d,e). Of these metabolites, *N*-acetyl aspartate has an amide

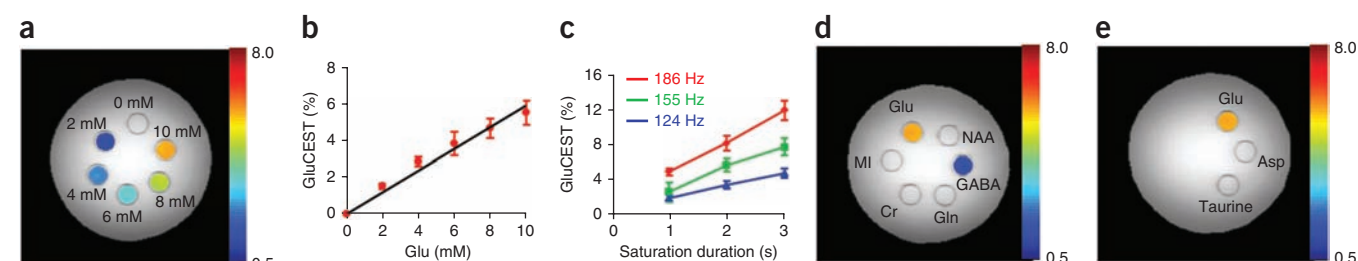


Figure 2 GluCEST images at 7T of a phantom consisting of test tubes with different concentrations of glutamate (pH 7.0) immersed in a beaker containing PBS. All the experiments were performed at 37 °C. (a) GluCEST contrast color-coded on the original CEST image (3 p.p.m.), acquired with application of saturation pulse train with $B_{1rms} = 155$ Hz (3.6 μT) for 2 s. Color bar represents percentage GluCEST contrast. (b) Linear dependence ($R^2 = 0.97$) of GluCEST effect on glutamate (Glu) concentration with a slope of $\sim 0.6\%$ per mM glutamate. (c) GluCEST dependence on B_{1rms} and duration of the saturation pulse. (d,e) CEST images of a phantom consisting of test tubes immersed in a beaker containing PBS, with solution of the different metabolites (pH 7) at their physiological concentrations. Glu, 10 mM glutamate; GABA, 2 mM GABA; NAA, 10 mM *N*-acetyl aspartate; Gln, 2 mM glutamine; Asp, 2 mM aspartate; 2 mM taurine; Cr, 6 mM creatine and MI, 10 mM myo-inositol. The CEST contrast color-coded on the original CEST images (3 p.p.m.), showing substantial CEST contrast from glutamate ($\sim 6\%$), with $\sim 1\%$ from GABA, $< 0.5\%$ from creatine and no contrast from other metabolites. Color bar represents percentage CEST contrast. The error bars represent s.d. from repeated experiments.



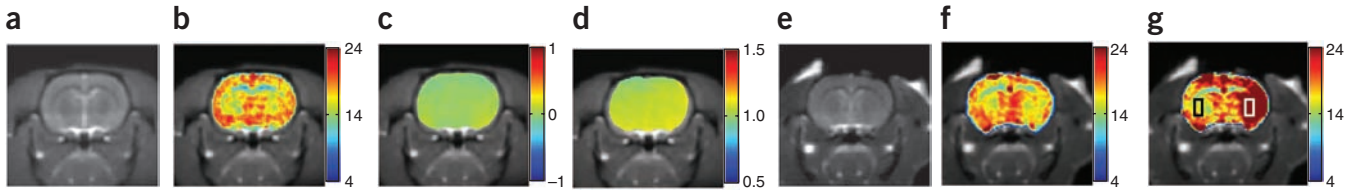


Figure 3 GluCEST mapping of healthy and ischemic rat brain. (a–d) Anatomic image, GluCEST map, local static magnetic field (B_0) and radiofrequency field (B_1) maps of healthy rat brain slice, respectively. Clear differences of GluCEST contrast in gray matter and white matter regions can be seen. (e) MCAO rat brain anatomic proton image. (f,g) GluCEST maps acquired at 1 h and 4.5 h after the induction of stroke. (h) The GluCEST contrast versus time after MCAO at regions of interest within the rectangular areas shown in g. (i) The GluCEST asymmetry plots from the contralateral side (blue curve) and ipsilateral side (red curve) at 4.5 h after occlusion. (j) The contralateral and ipsilateral sides of MCAO rat brain data acquired at 4.7 T at 4 h after occlusion and 1 h post-mortem. (Panel j reprinted from ref. 18.). The error bars represent s.d. from repeated experiments.

proton, but at neutral pH it did not show any CEST effect. Choline does not have any exchangeable protons. Myo-inositol has exchangeable hydroxyl protons and showed a CEST effect at ≤ 1 p.p.m., which did not extend beyond 2 p.p.m. at neutral pH. Creatine has amine protons that showed a CEST effect around 1.8 p.p.m. at physiological pH. However, its contribution to the GluCEST effect at 3 p.p.m. was also not appreciable ($<0.5\%$). No contributions to GluCEST were observed from aspartate, glutamine and taurine at their physiological concentrations under the experimental conditions used, possibly because of unfavorable exchange rates and differences in the chemical shifts of their amine protons.

Rat studies

In healthy rat brain, the gray matter and white matter were clearly separated in the GluCEST, with a contrast ratio of ~ 1.6 (Fig. 3a–d). The glutamate amine exchange rate measured in healthy rat brain was $\sim 2,000 \pm 500 \text{ s}^{-1}$ (Supplementary Methods), which is well within the slow to intermediate exchange regime at 7T.

GluCEST obtained from a rat brain following middle cerebral artery occlusion (MCAO) stroke showed significant differences between ipsilateral and contralateral sides (Fig. 3e–h). The ipsilateral side

demonstrated an $\sim 100\%$ increase in GluCEST at 4.5 h after MCAO (Fig. 3h). The z-spectral asymmetry plots from the MCAO brain reported here showed an elevation of CEST, whereas z-spectra from a previously reported MCAO study in the rat brain¹⁸ have shown decreased amide proton CEST effects from the ipsilateral side compared with the contralateral side (Fig. 3i,j). In addition, amide proton CEST asymmetry plots have shown negative values at 3 p.p.m.¹⁸, whereas our GluCEST showed positive values. This is because of key differences in the amide proton CEST and GluCEST experimental conditions. Because of low exchange rates ($\sim 30 \text{ s}^{-1}$) in amide proton CEST, a lower saturation pulse amplitude (root mean square B_1 ($B_{1\text{rms}}$) = 50 Hz (1.2 μT)) and longer duration (~ 6 s) were used in the earlier study. However, owing to the higher glutamate exchange rate, higher $B_{1\text{rms}}$ and shorter duration were used in this study ($B_{1\text{rms}}$ = 155 Hz (3.6 μT) and 1 s).

Literature studies have shown that in the MCAO model of ischemia, extracellular glutamate levels ($\sim 1\text{--}2 \mu\text{M}$ basal value)²⁶ increase substantially to $\sim 0.2 \text{ mM}$ (ref. 27). However, the total glutamate concentration (extracellular and intracellular) may remain unaltered. In addition, although extracellular concentrations (in μM) of other molecules such as GABA, aspartate, adenosine and taurine also increase²⁸, their concentration changes are too small to account for the observed GluCEST effects.

In the MCAO model, it is also well established that the magnitude of pH decrease expected over a 4-h period is ~ 0.5 units¹⁸. In addition to pH, other factors that potentially affect GluCEST during stroke are changes to the water content, water spin-spin relaxation time (T_2) and magnetization transfer ratio (MTR). It has been reported that in

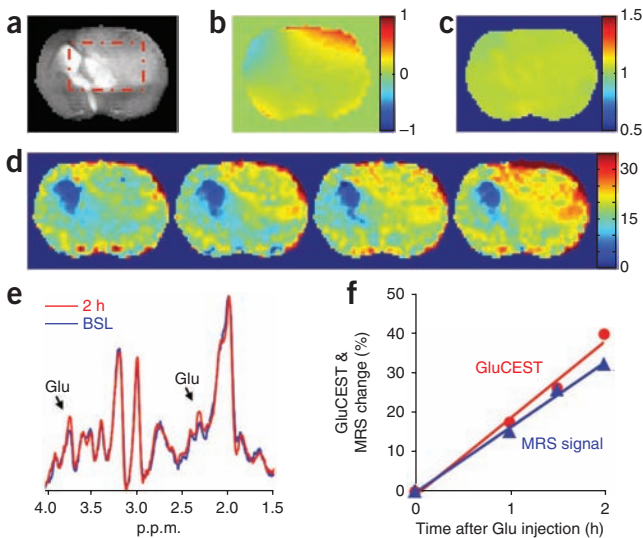


Figure 4 GluCEST images and ^1H MRS of rat brain with a tumor, before and after injection of glutamate. (a) Rat brain anatomic proton image demonstrating the tumor and a rectangular region of interest. (b) B_0 map of the rat brain, which shows about ± 0.5 p.p.m. variation. Color bar is in units of p.p.m. (c) B_1 map (the ratio of $B_1/B_{1\text{ref}}$, unitless) of the rat brain showing a fairly uniform B_1 field. (d) GluCEST maps of the rat brain acquired before injection (BSL) and at 1, 1.5 and 2.0 h after the injection of glutamate solution. Color bars represent percentage GluCEST contrast. (e) Stacked stimulated echo acquisition mode (STEAM) localized ^1H MRS data (in arbitrary MR units) acquired at baseline and at 2 h after the glutamate (Glu) injection (arrows). (f) Time course of GluCEST and the 2.3 p.p.m. glutamate peak integral normalized with the values of pre-injection from regions of interest within the rectangular areas shown in a.



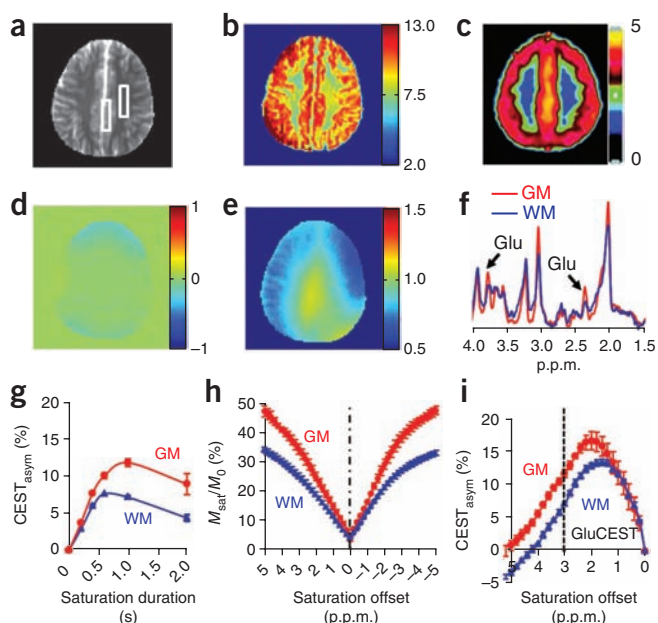


Figure 5 GluCEST imaging and ^1H MRS from a healthy human brain acquired at 7T. (a) Anatomic proton image of the axial slice. (b) B_1 and B_0 corrected GluCEST contrast map. Color bar represents percentage GluCEST contrast. (c) Map of distribution volumes (DVs) of metabotropic glutamate receptor subtype 5 from a PET image (reprinted from ref. 31 with permission of the Society of Nuclear Medicine). (d) B_0 map and (e) B_1 map corresponding to the slice in a. (f) ^1H MRS spectra obtained from regions of interest of gray matter and white matter shown in a. These spectra (in arbitrary MR units) show higher amplitude of glutamate $-\text{CH}_2$ resonance (2.3 p.p.m.) and $-\text{CH}$ resonance (3.75 p.p.m.) in gray matter than that in white matter. (g) Saturation pulse duration dependence of GluCEST data from human brain. The GluCEST reaches a maximum at a saturation duration of ~ 1 s and decreases with further increase in duration. (h,i) The z-spectra and corresponding asymmetry plots from human gray matter and white matter regions. The GluCEST at 3 p.p.m. (dotted line in i) is $\sim 11\%$ from gray matter and $\sim 7\%$ from white matter. Glu, glutamate; GM, gray matter; WM, white matter.

the MCAO model, the T_2 of water is elevated by ~ 20 to 40%, MTR is reduced by $\sim 20\%$ and total water content may be changed by ~ 2 to 4%^{18,29}. These changes in T_2 , MTR and water content are expected to account for only minor changes in GluCEST.

In polypeptide solutions in PBS, the CEST effect from amine and amide protons has been shown to decrease with decreasing pH in the pH 7.3–5.0 range³⁰. In contrast, GluCEST increased here by almost 100% during MCAO ischemia. This increase in GluCEST is consistent with the pH-dependent GluCEST behavior observed in glutamate phantoms at physiological concentrations and temperature, and it suggests that the elevated GluCEST in the ipsilateral side of MCAO model is predominantly because of lower pH.

In healthy brain, glutamate does not cross the blood-brain barrier (BBB); however, the compromised BBB in a tumor model provides a means of demonstrating glutamate modulation, where GluCEST should change approximately linearly with the concentration of glutamate. To demonstrate that the GluCEST measured *in vivo* is specific to glutamate, we performed GluCEST and ^1H MRS studies in a rat brain with a tumor before and after the intravenous injection of glutamate solution (Fig. 4a–f). GluCEST maps obtained at three time points after injection showed that there was a notable increase in GluCEST in the tumor, with a concomitant similar elevation in the ^1H MRS of glutamate.

In vivo human brain study

A GluCEST map obtained from a healthy human brain (Fig. 5) showed a gray matter and white matter distribution pattern similar to a published positron emission tomography (PET) map of the metabotropic glutamate receptor subtype 5 (mGluR5) (Fig. 5c and ref. 31). Concentrations of glutamate derived from the ^1H MRS data (5.9 ± 0.5 mM for white matter and 9.4 ± 1.4 mM for gray matter) were also consistent with the GluCEST from the same regions of interest (ROIs) (Fig. 5a,b,f).

In human brain, the gray matter and white matter GluCEST contrast was the highest at a saturation pulse length of ~ 1 s (Fig. 5g). The z-spectra and CEST asymmetry curves from gray matter and white matter regions of the brain were rather broad and showed a maximum CEST contrast at ~ 2 p.p.m. (Fig. 5i,j). The broadness in asymmetry plots may be partly due to (i) the glutamate exchange-induced chemical shift averaging effect that shifts the line toward water resonance and (ii) an additional potential contribution from creatine³². Similar results were observed in three volunteers. The intrasubject coefficient of variation of measured GluCEST was $< 5\%$.

The GluCEST maps obtained in healthy human brain reflected the known regional variation of physiological concentrations of glutamate^{33,34}. Because ^1H MRS data are highly specific to the concentration of glutamate, the observed strong correlation between GluCEST ratio from gray matter and white matter ROIs (1.6 ± 0.2) with the glutamate concentration ratio from ^1H MRS data in the same ROIs (1.6 ± 0.1) provided additional confirmation that the observed GluCEST in the human brain is predominantly due to glutamate. We estimate that ~ 70 – 75% of the observed GluCEST was from glutamate (Supplementary Table 1).

DISCUSSION

These findings provide what is to our knowledge the first evidence that GluCEST can be used for noninvasive imaging of glutamate concentrations, with excellent spatial and temporal resolution. In addition to its role as the predominant excitatory neurotransmitter in the brain, glutamate also serves as a metabolic intermediate, and it is likely that GluCEST detects both of these pools.

Although the gray matter to white matter GluCEST contrast ratio in humans, as well as in healthy rat brains, is very similar ($\sim 1.6 \pm 0.2$), the GluCEST magnitude in the rat brain is higher than that in the human brain because of higher strength magnetic fields (9.4T in rats versus 7T in humans), continuous saturation pulses used on rats (constrained by the scanner software) and lower direct water saturation at 9.4T in rats compared with 7T in humans. Because of the fast exchange rate of glutamate amine protons, the slow to intermediate exchange rate condition is not fulfilled at lower-field whole-body clinical scanners ($\leq 3\text{T}$), and, hence, these studies are expected to have poor sensitivity at these fields.

Potential contributions of MTR asymmetry to GluCEST, caused by the bound pool of water from rigid macromolecules in biological tissues, cannot be excluded. MTR asymmetry effects³⁵, if any, would compete with the GluCEST effect and would lead to an underestimation of actual GluCEST levels. Indeed, the simulated MTR asymmetry (-0.14% in gray matter and -0.22% in white matter) (Supplementary Table 1 and Supplementary Discussion) indicates that its contribution to the observed GluCEST is likely to be negligibly small.

Here SAR issues at 7T limit the observed GluCEST sensitivity in humans. However, saturation pulse power, duration, pulse shapes and readout sequences, in conjunction with multichannel RF coils, could be further optimized to enhance GluCEST effects within

FDA guidelines for SAR deposition. The glutamate contribution to GluCEST may have slight variations per site, depending on the RF coil or static field strength used, and future work should evaluate these contributions for specific experimental conditions.

Studies at ultrahigh fields beyond 7T would further enhance the sensitivity of GluCEST, albeit with additional challenges in dealing with SAR deposition. For proof-of-principle purposes, we used only a single slice with a two-dimensional imaging sequence. However, it would be relatively straightforward to implement a three-dimensional acquisition of GluCEST maps.

In summary, GluCEST detection is feasible in the human brain at ultrahigh field (7T) without exceeding the allowed limits on SAR. About 70–75% of the observed CEST is from glutamate, with the remaining 25–30% coming from creatine, GABA and other macromolecules. Despite small contamination from other molecules *in vivo*, the GluCEST method can be used to study relative changes in glutamate through endogenous or exogenous glutamate modulation *in vivo*. This method provides noninvasive, nonradioactive and high spatial and temporal resolution imaging of relative changes in glutamate for use in both human subjects and preclinical models. Further, the exquisite sensitivity of GluCEST to changes in pH could potentially be used as a pH marker in evolving stroke and tumors. Future studies using this approach may provide new insights into glutamate function and demonstrate its potential as a biomarker for the diagnosis and treatment of CNS disorders.

METHODS

Methods and any associated references are available in the online version of the paper at <http://www.nature.com/naturemedicine/>.

Note: Supplementary information is available on the Nature Medicine website.

ACKNOWLEDGMENTS

We gratefully acknowledge stimulating discussions with R.N. Bryan, M.D. Schnall, J.D. Glickson and W.S. Englander. We thank W. Liu and S. Pickup for their technical assistance in using the 9.4 T research scanners, W.R.T. Witschey for technical support, P. Waghay for experimental help and D. Reddy, K. Nath and T. Hiraki for help with animal models. This work was carried out at a US National Institutes of Health-supported resource, with funding from P41RR002305.

AUTHOR CONTRIBUTIONS

K.C., M.H. and A.S. designed and performed experiments, analyzed data and wrote the manuscript; F.K. did experiments and helped with manuscript editing; J.H.G. helped with rat studies and manuscript editing; J.A.D. advised on neuroimaging aspects and contributed to the manuscript editing; H.H. provided pulse sequence design and technical guidance and contributed to the manuscript writing; R.R. provided conception and overall experimental design and contributed to manuscript writing and editing.

COMPETING FINANCIAL INTERESTS

The authors declare no competing financial interests.

Published online at <http://www.nature.com/naturemedicine/>.

Reprints and permissions information is available online at <http://www.nature.com/reprints/index.html>.

1. Petroff, O.A. GABA and glutamate in the human brain. *Neuroscientist* **8**, 562–573 (2002).
2. Harrison, P.J. Metabotropic glutamate receptor agonists for schizophrenia. *Br. J. Psychiatry* **192**, 86–87 (2008).
3. Paul, I.A. & Skolnick, P. Glutamate and depression: clinical and preclinical studies. *Ann. NY Acad. Sci.* **1003**, 250–272 (2003).
4. Chojnacka-Wójcik, E., Klodzinska, A. & Pilc, A. Glutamate receptor ligands as anxiolytics. *Curr. Opin. Investig. Drugs* **2**, 1112–1119 (2001).
5. Rothman, D.L., Petroff, O.A., Behar, K.L. & Mattson, R.H. Localized ¹H NMR measurements of gamma-aminobutyric acid in human brain *in vivo*. *Proc. Natl. Acad. Sci. USA* **90**, 5662–5666 (1993).

6. Ryner, L.N., Sorenson, J.A. & Thomas, M.A. 3D localized 2D NMR spectroscopy on an MRI scanner. *J. Magn. Reson. B.* **107**, 126–137 (1995).
7. Ryner, L.N., Sorenson, J.A. & Thomas, M.A. Localized 2D J-resolved ¹H MR spectroscopy: strong coupling effects in vitro and in vivo. *Magn. Reson. Imaging* **13**, 853–869 (1995).
8. Hurd, R. *et al.* Measurement of brain glutamate using TE-averaged PRESS at 3T. *Magn. Reson. Med.* **51**, 435–440 (2004).
9. Gottschalk, M., Lamalle, L. & Segebarth, C. Short-TE localised ¹H MRS of the human brain at 3 T: quantification of the metabolite signals using two approaches to account for macromolecular signal contributions. *NMR Biomed.* **21**, 507–517 (2008).
10. Petroff, O.A., Mattson, R.H. & Rothman, D.L. Proton MRS: GABA and glutamate. *Adv. Neurol.* **83**, 261–271 (2000).
11. Forsen, S. & Hoffman, R.A. Study of moderately rapid chemical exchange reactions by means of nuclear magnetic double resonance. *J. Chem. Phys.* **39**, 2892–2901 (1963).
12. Ward, K.M., Aletras, A.H. & Balaban, R.S. A new class of contrast agents for MRI based on proton chemical exchange dependent saturation transfer (CEST). *J. Magn. Reson.* **143**, 79–87 (2000).
13. Sherry, A.D. & Woods, M. Chemical exchange saturation transfer contrast agents for magnetic resonance imaging. *Annu. Rev. Biomed. Eng.* **10**, 391–411 (2008).
14. Woessner, D.E., Zhang, S., Merritt, M.E. & Sherry, A.D. Numerical solution of the Bloch equations provides insights into the optimum design of PARACEST agents for MRI. *Magn. Reson. Med.* **53**, 790–799 (2005).
15. Zhou, J. & van Zijl, P.C. Chemical exchange saturation transfer imaging and spectroscopy. *Prog. Nucl. Magn. Reson. Spectrosc.* **48**, 109–136 (2006).
16. Jones, C.K. *et al.* Amide proton transfer imaging of human brain tumors at 3T. *Magn. Reson. Med.* **56**, 585–592 (2006).
17. Englander, S.W., Downer, N.W. & Teitelbaum, H. Hydrogen exchange. *Annu. Rev. Biochem.* **41**, 903–924 (1972).
18. Zhou, J., Payen, J.F., Wilson, D.A., Traystman, R.J. & van Zijl, P.C. Using the amide proton signals of intracellular proteins and peptides to detect pH effects in MRI. *Nat. Med.* **9**, 1085–1090 (2003).
19. Sun, P.Z., Zhou, J., Sun, W., Huang, J. & van Zijl, P.C. Detection of the ischemic penumbra using pH-weighted MRI. *J. Cereb. Blood Flow Metab.* **27**, 1129–1136 (2007).
20. van Zijl, P.C., Jones, C.K., Ren, J., Malloy, C.R. & Sherry, A.D. MRI detection of glycogen *in vivo* by using chemical exchange saturation transfer imaging (glycoCEST). *Proc. Natl. Acad. Sci. USA* **104**, 4359–4364 (2007).
21. Ling, W., Regatte, R.R., Navon, G. & Jerschow, A. Assessment of glycosaminoglycan concentration *in vivo* by chemical exchange-dependent saturation transfer (gagCEST). *Proc. Natl. Acad. Sci. USA* **105**, 2266–2270 (2008).
22. Gilad, A.A. *et al.* Artificial reporter gene providing MRI contrast based on proton exchange. *Nat. Biotechnol.* **25**, 217–219 (2007).
23. Haris, M., Cai, K., Singh, A., Hariharan, H. & Reddy, R. *In vivo* mapping of brain myo-inositol. *Neuroimage* **54**, 2079–2085 (2011).
24. McConnell, H.M. Reaction rates by nuclear magnetic resonance. *J. Chem. Phys.* **28**, 430–431 (1958).
25. Chu, W.J. *et al.* Is the intracellular pH different from normal in the epileptic focus of patients with temporal lobe epilepsy? A ³¹P NMR study. *Neurology* **47**, 756–760 (1996).
26. Dávalos, A., Shuaib, A. & Wahlgren, N.G. Neurotransmitters and pathophysiology of stroke: evidence for the release of glutamate and other transmitters/mediators in animals and humans. *J. Stroke Cerebrovasc. Dis.* **9**, 2–8 (2000).
27. Kiewert, C., Mdzinarishvili, A., Hartmann, J., Bickel, U. & Klein, J. Metabolic and transmitter changes in core and penumbra after middle cerebral artery occlusion in mice. *Brain Res.* **1312**, 101–107 (2010).
28. Melani, A. *et al.* Striatal outflow of adenosine, excitatory amino acids, gamma-aminobutyric acid, and taurine in awake freely moving rats after middle cerebral artery occlusion: correlations with neurological deficit and histopathological damage. *Stroke* **30**, 2448–2454 discussion 2455 (1999).
29. Tuor, U.I. *et al.* Differential progression of magnetization transfer imaging changes depending on severity of cerebral hypoxic-ischemic injury. *J. Cereb. Blood Flow Metab.* **28**, 1613–1623 (2008).
30. McMahan, M.T. *et al.* New “multicolor” polypeptide diamagnetic chemical exchange saturation transfer (DIACEST) contrast agents for MRI. *Magn. Reson. Med.* **60**, 803–812 (2008).
31. Ametamey, S.M. *et al.* Human PET studies of metabotropic glutamate receptor subtype 5 with 11C-ABP688. *J. Nucl. Med.* **48**, 247–252 (2007).
32. Sun, P.Z. & Sorensen, A.G. Imaging pH using the chemical exchange saturation transfer (CEST) MRI: Correction of concomitant RF irradiation effects to quantify CEST MRI for chemical exchange rate and pH. *Magn. Reson. Med.* **60**, 390–397 (2008).
33. Michaelis, T., Merboldt, K.D., Bruhn, H., Hanicke, W. & Frahm, J. Absolute concentrations of metabolites in the adult human brain *in vivo*: quantification of localized proton MR spectra. *Radiology* **187**, 219–227 (1993).
34. Choi, I.Y., Lee, S.P., Merkle, H. & Shen, J. *In vivo* detection of gray and white matter differences in GABA concentration in the human brain. *Neuroimage* **33**, 85–93 (2006).
35. Hua, J. *et al.* Quantitative description of the asymmetry in magnetization transfer effects around the water resonance in the human brain. *Magn. Reson. Med.* **58**, 786–793 (2007).



ONLINE METHODS

MRI scans. All the phantom and human MRI studies were performed in a 7T Siemens whole body MRI scanner (Siemens Medical Systems) with a circularly polarized RF coil. All phantoms were prepared in PBS, and all the experiments were performed at 37 °C. Rat experiments were performed in a 9.4T Varian scanner (Agilent Technologies).

Phantom imaging. A new pulse sequence was written to use a frequency selective saturation pulse followed by a segmented RF spoiled gradient echo (GRE) readout sequence. The imaging parameters were as follows: slice thickness = 10 mm, flip angle = 10°, TR = 5.6 ms, TE = 2.7 ms, field of view (FOV) = 120 × 120 mm², matrix size = 192 × 192, with one saturation pulse and 64 segments acquired every 15 s. CEST images were collected using a saturation pulse at a B_{1rms} of 155 Hz (3.6 μT) and 2-s duration and frequencies from -5 to 5 p.p.m. in steps of 0.2 p.p.m.

Rat experiments. All rat experiments were performed according to an approved University of Pennsylvania Institutional Animal Care and Use Committee protocol. For healthy and MCAO studies, Sprague-Dawley male rats (265–315 g, Charles River Laboratories) were used, and, for tumor model studies, female Fisher rats (130–150 g, Charles River Laboratories) were used. Both MCAO and tumor models were prepared as described in the **Supplementary Methods**.

Rat imaging and spectroscopy. Healthy ($n = 2$), MCAO ($n = 3$) and tumor-bearing rats ($n = 3$) were imaged using a 35-mm-diameter quadrature RF coil (m2m Imaging Corp.). Animals were kept under anesthesia (1.5% isoflurane in 1 l min⁻¹ oxygen) and kept warm with the warm air from a heater. Respiration and body temperature were monitored using an MRI-compatible small animal monitoring system (SA Instruments). CEST imaging was performed using a frequency selective continuous wave saturation pulse followed by a segmented GRE readout sequence. The imaging parameters were FOV = 35 × 35 mm², slice thickness = 2 mm, flip angle = 15°, TR = 6.2 ms, TE = 2.9 ms, matrix size = 128 × 128 and number of averages = 2, with one saturation pulse and 32 segments acquired every 4 s. CEST images were collected using a 1-s-long rectangular saturation pulse at B_{1rms} of 250 Hz (5.9 μT) at multiple frequencies in the range -5 to 5 p.p.m. with a step size of 0.2 p.p.m. Data for B₁ and B₀ maps were also acquired. *In vivo* exchange rate in healthy rat brain at 9.4T was measured using a previously described method¹⁴. In tumor-bearing rats, along with GluCEST data, water suppressed STEAM single voxel spectra were obtained with the following parameters: voxel size = 11 × 8 × 5 mm³, spectral width = 4 kHz, number of points = 2048, average = 128, TE = 8 ms and TR = 6 s. After collecting the baseline CEST map and ¹H MRS, the rats were injected

with 2.5 ml of 100 mM glutamate solution through the tail vein. CEST and ¹H MRS data were gathered periodically for ~2 h after the injection.

Human studies. The studies were conducted under an approved Institutional Review Board protocol of the University of Pennsylvania. GluCEST imaging and z-spectrum acquisitions of human brain at 7T were performed on three normal volunteers (male, ages 27–35 years). Informed consent from each volunteer was obtained after explaining the study protocol. Brain CEST imaging was performed with the application of the same imaging protocol as described for the phantoms except with a larger FOV (240 × 240 mm²), averages (4) and matrix size (128 × 128). Original CEST images and GluCEST contrast maps were corrected for B₀ and B₁ inhomogeneities (**Supplementary Methods**). Water suppressed ¹H MRS were obtained from gray matter and white matter regions using the standard point resolved spectroscopy (PRESS)³⁶ localization technique with the following parameters: voxel size = 10 × 40 × 10 mm³, spectral width = 4 kHz, number of points = 2,048, average = 100, TE = 16 ms, and TR = 3 s.

Data processing. All image processing and data analysis was performed using in-house written programs in MATLAB (version 7.5, R2007b). Acquired images were corrected for B₀ and B₁ inhomogeneities, and z-spectra were obtained from these images by plotting the normalized image intensity as a function of resonance offset of saturation pulse for each sample. CEST contrast was calculated with the following equation³⁷:

$$CEST_{\text{asym}}(\Delta\omega) = \frac{M_{\text{sat}}(-\Delta\omega) - M_{\text{sat}}(\Delta\omega)}{M_{\text{sat}}(-\Delta\omega)} \quad (1)$$

where $M_{\text{sat}}(\pm\Delta\omega)$ represent the magnetizations obtained with saturation at a positive or negative $\Delta\omega$ offset from the water resonance. $CEST_{\text{asym}}$ contrast at 3 p.p.m. is referred to as GluCEST. ¹H MRS spectra were fitted using nonlinear least-squares methods with Gaussian functions. Peak integrals were calculated and normalized with a non-water-suppressed proton signal for calculating glutamate concentrations *in vivo*.

Additional methods. Detailed methodology is described in the **Supplementary Methods**.

36. Bottomley, P.A. Spatial localization in NMR spectroscopy *in vivo*. *Ann NY Acad. Sci* **508**, 333–348 (1987).

37. Liu, G., Gilad, A.A., Bulte, J.W., van Zijl, P.C. & McMahon, M.T. High-throughput screening of chemical exchange saturation transfer MR contrast agents. *Contrast Media Mol. Imaging* **5**, 162–170 (2010).